Chapter 1

Introduction

The sun has been an object of scientific interest since the time of the ancient Greeks and an object of wonder since long before then. It is the centre piece of the solar system and its varied and powerful characteristics impinge markedly on life on earth, making detailed study of its processes both a useful and important effort. The earth exists in a delicate balance with a sensitive dependence on the behaviour of the sun. Any closer and it would be too hot for life. Any further away and it would be too cold. Long term solar cycles produce global warming and ice ages and planets that lack a protective magnetosphere have their atmospheres stripped away by the solar wind. This process is underway on Venus which has a solar wind induced comet-like tail that stretches as far as earth. On smaller timescales, coronal mass ejections, when oriented appropriately, are capable of simultaneously producing the beautiful aurorae and destroying satellites and power grids.

In these days when the depletion of fossil fuels and atmospheric pollution are critical issues and the potential of renewable energy sources is of key interest, the sun is an obvious choice of generator providing, for all practical purposes, limitless energy. The effective harnessing of such energy will benefit greatly from an increased understanding of the sun. Solar physics research also presents an opportunity to study a naturally magnetically confined plasma environment. It therefore provides useful knowledge and insight for the development of magnetically confined laboratory fusion plasmas, which are being developed around the world as abundant sources of

power.

The sun is a fairly average star and its proximity to the earth allows it to be resolved into subregions – other stars can only be seen as single objects. Consequently study of the sun provides much information pertinent to stellar physics.

The sun is an extremely diverse and dynamic creature which poses a whole host of rich physical questions and only the basics of solar physics are understood to any depth. The Solar and Heliospheric Observatory (SOHO - Domingo et al., 1995) is a joint NASA (National Aeronautics and Space Administration) and ESA (European Space Agency) spacecraft situated in orbit round the sun-earth L1-Lagrange point – the point where the gravitational force due to the sun is balanced by that of the earth. It has a payload of twelve instruments designed collectively to address three of the main unanswered questions in solar physics. Namely,

1. What is the detailed structure of the solar interior?

2. How is the solar corona heated?

3. How is the solar wind accelerated?

To address the question of coronal heating, SOHO carries six solar atmosphere remote sensing instruments, one of which is the Solar Ultraviolet Measurements of Emitted Radiation (SUMER) spectrometer (Wilhelm et al., 1995), data from which is discussed here.

Fig. 1.1 shows a model of the temperature structure of the solar atmosphere. The photosphere (heights $<$ 0 km) is relatively dense and cool ($\sim$ 6000K). Above the photosphere is a narrow layer called the chromosphere which spans a temperature range from the temperature minimum of $\sim$ 4,000 K just above the photosphere, up to $\sim$ 20,000 K at $\sim$ 2000km. Between the chromosphere and the corona a transition region of uncertain structure exists which spans the region $\sim$ 20,000 $\rightarrow$ $\sim$ 2,000,000K. Above the transition region is the corona which extends to many solar radii at a temperature of $\sim$ 2,000,000K.

The images shown in figs 1.2, 1.3 and 1.4 give some indication of the dynamic nature of the solar atmosphere. If the dynamics are to be understood it is necessary

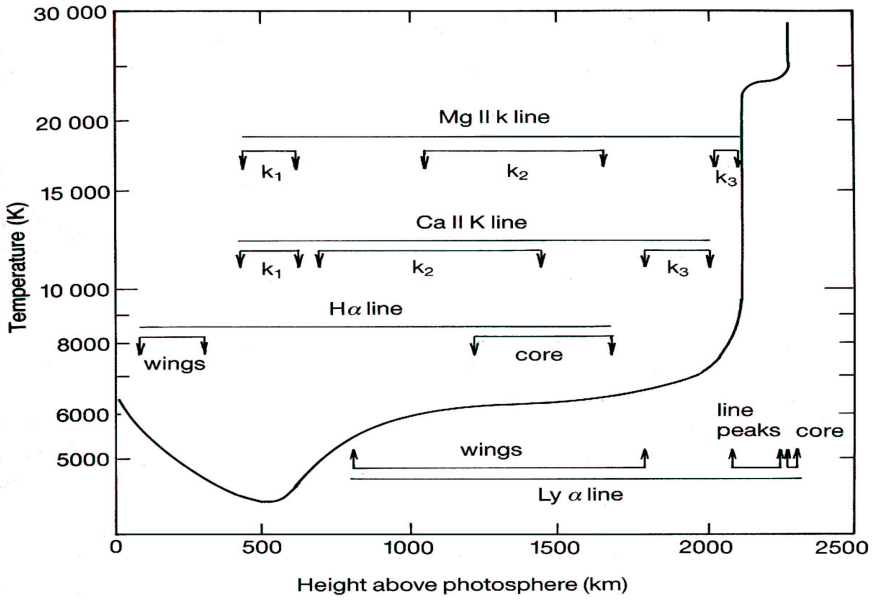

Figure 1.1: The variation in temperature with height in the solar atmosphere up to the transition region based on the hydrostatic equilibrium model of Vernazza et al. (1981). (Taken from Phillips, 1992).

to first probe the atmospheric and temperature structures of the *quiet sun* – i.e. the non-active sun – though, as the recent SOHO data bears testimony, even the quiet sun is dynamic on timescales less than that of ionisation equilibrium (Brooks et al., 1998). This thesis seeks to develop methods useful for both the diagnosis and modelling of plasma structure from observations of *optically thick* spectra.

1.1 The solar chromosphere and transition region

The regions of the solar atmosphere which are of particular interest in this work are the *chromosphere* and the *transition region* (TR). The solar chromosphere is a narrow part of the solar atmosphere visible during an eclipse or with special observing techniques. Its main characteristics are a rise in temperature with height and a complex dynamic structure. Hα and calcium H and K line spectroheliograms (eg. fig 1.2) of the sun show that the chromosphere is a highly non-uniform, structured region of the solar

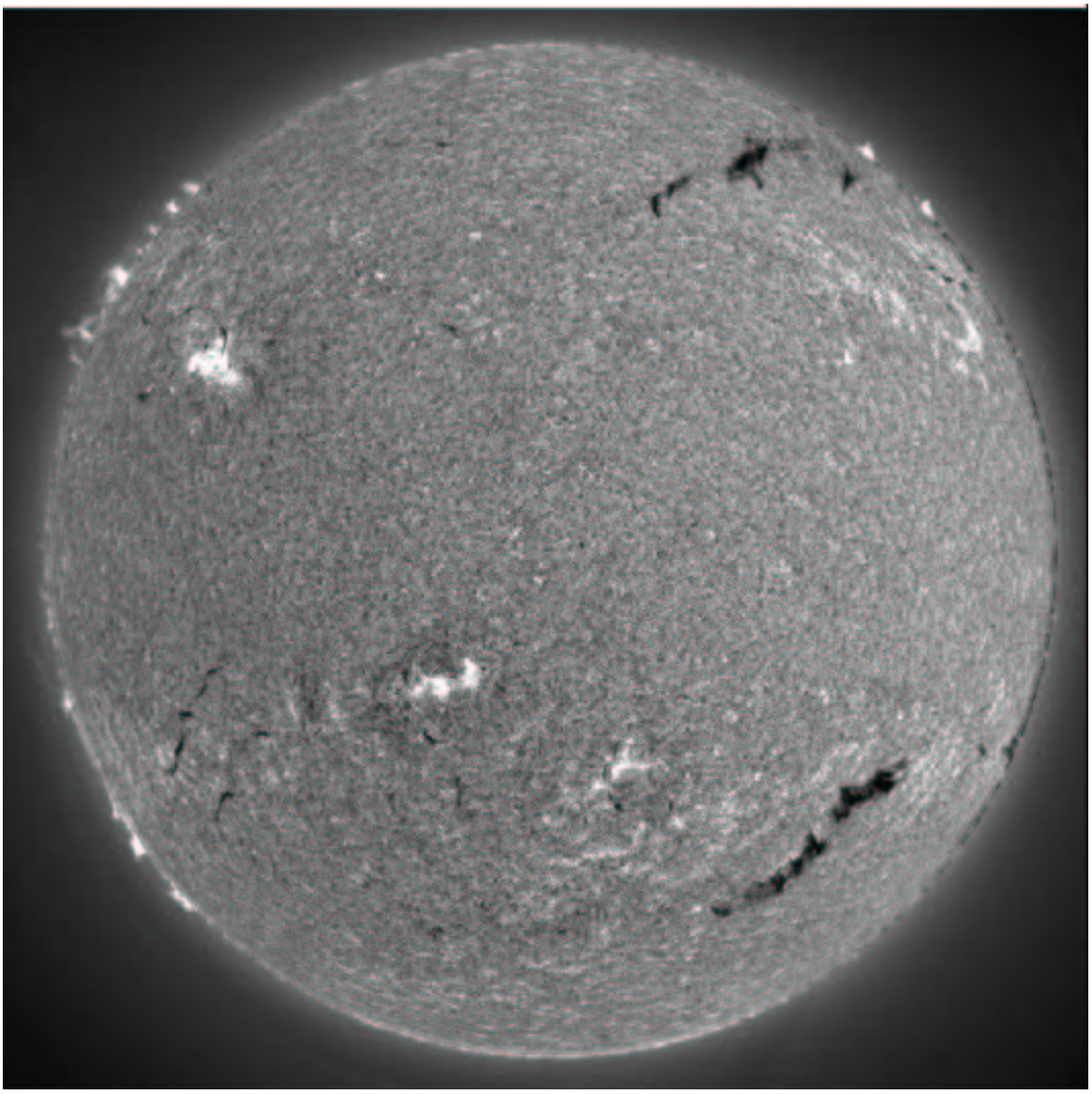

Figure 1.2: Image of the solar disk in hydrogen Hα at 6563 Å revealing the lower chromosphere. Several active regions are evident as well as many prominence filaments (see sec. 1.1.2). A number of prominences are visible at the limb.

atmosphere. In fig. 1.2 large bright zones called *active regions* are visible with bright patches in their vicinity known as *plages*. Evident also are long, dark structures called *filaments* (see sec. 1.1.2).

Fig. 1.3 shows the solar disk as seen in He II 304 Å which corresponds to a temperature of around 80,000 K. In this figure bright clumps that form a pattern can be seen. This pattern is known as the *chromospheric network* which is quite faint in quiet sun regions and more enhanced near active regions. An individual network cell is typically $\sim$ 30,000 km across and lasts about 1 day. The bright patches are called *floculi* or *coarse mottles*. A coarse mottle is made up of several bright *fine mottles* about 7000 km by 700 km, lasting about 1 day with both upward and downward velocities. Fine mottles are associated with *spicules* when viewed at the limb (see sec. 1.1.1).

Chromospheric features and the photospheric magnetic field are related on a small and a large scale. For example clumps of intra-network field within network cells are associated with bright cell points. This field appears at centres of supergranules and moves radially outwards to the supergranule edges where it either cancels or coalesces with the network field. On the larger scale, strong fields around sunspots are related to the plage structures.

Between the chromosphere and corona there is an even more narrow region known as the transition region (TR). This region has a complex structure with many features at or below the resolution limit of current observational instrumentation. Energy seems to be mostly supplied by thermal conduction and downflow of hot gas from the corona above. This means that dissipation of wave energy from the photosphere is not significant. This interpretation was questioned by Feldman & Lamming (1994). Measurements suggest that emission is due to tiny ($\sim$ 100 km) structures which are not resolvable. Feldman et al. postulate that much of the ultraviolet (UV) emission is due to these *unresolved fine structures* and only part is due to 'true' TR emission (i.e. chromosphere-corona interface).

Both the chromosphere and the TR are confined to the network which is steadily less sharply defined as temperature increases until the corona where it is not visible.

Plasma flow and photo-absorption affect spectral line profiles and so careful study

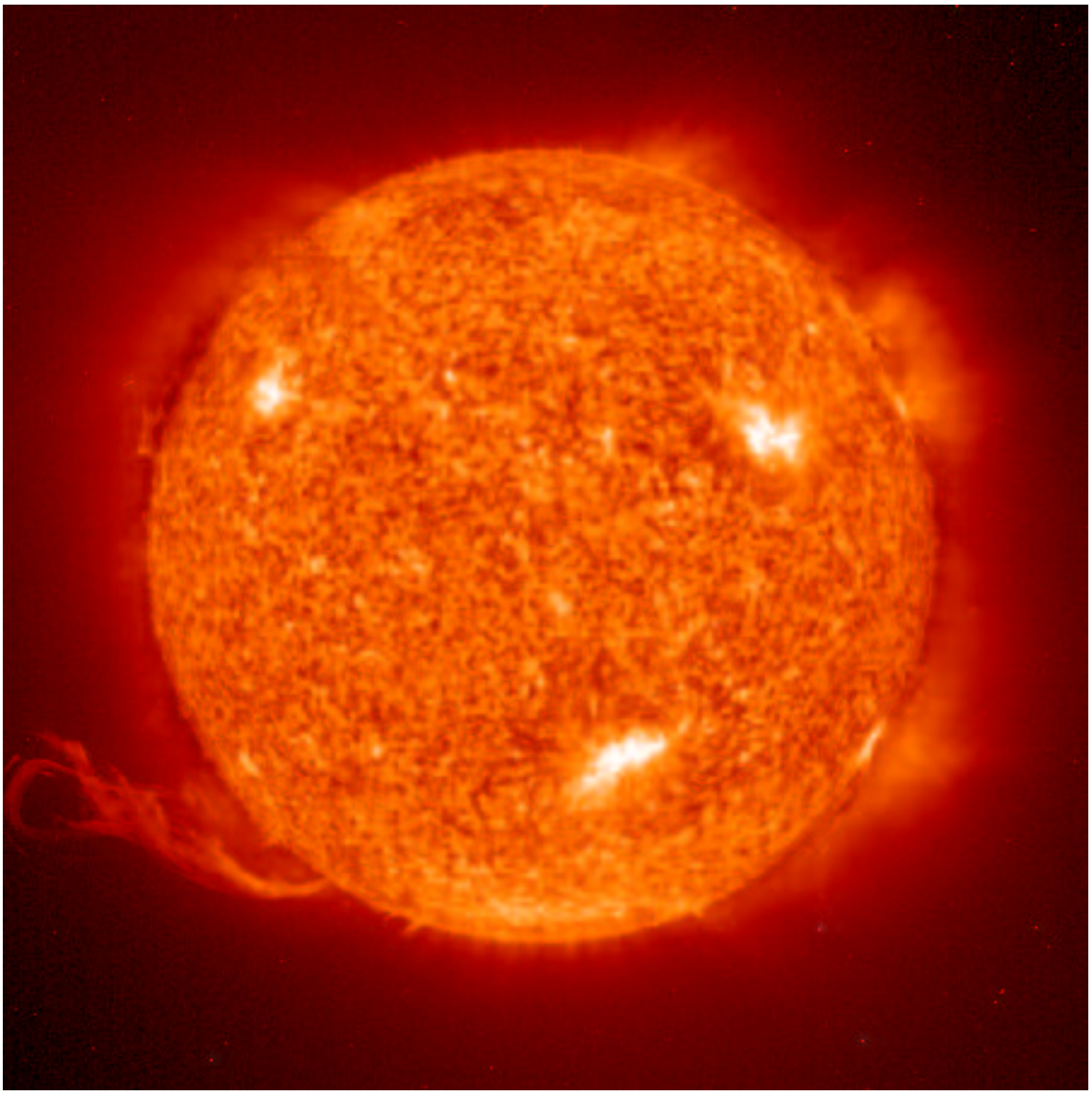

Figure 1.3: Image of the solar disk in He II 304 Å obtained using the Extreme-Ultraviolet Imaging Telescope (EIT) on SOHO, revealing the mid chromosphere ($\sim$ 80,000K). The bright patches on the disk are active regions which are situated above sunspots. The large structures above the limb are prominences and the spiky structures evident at the poles are macrospicules.

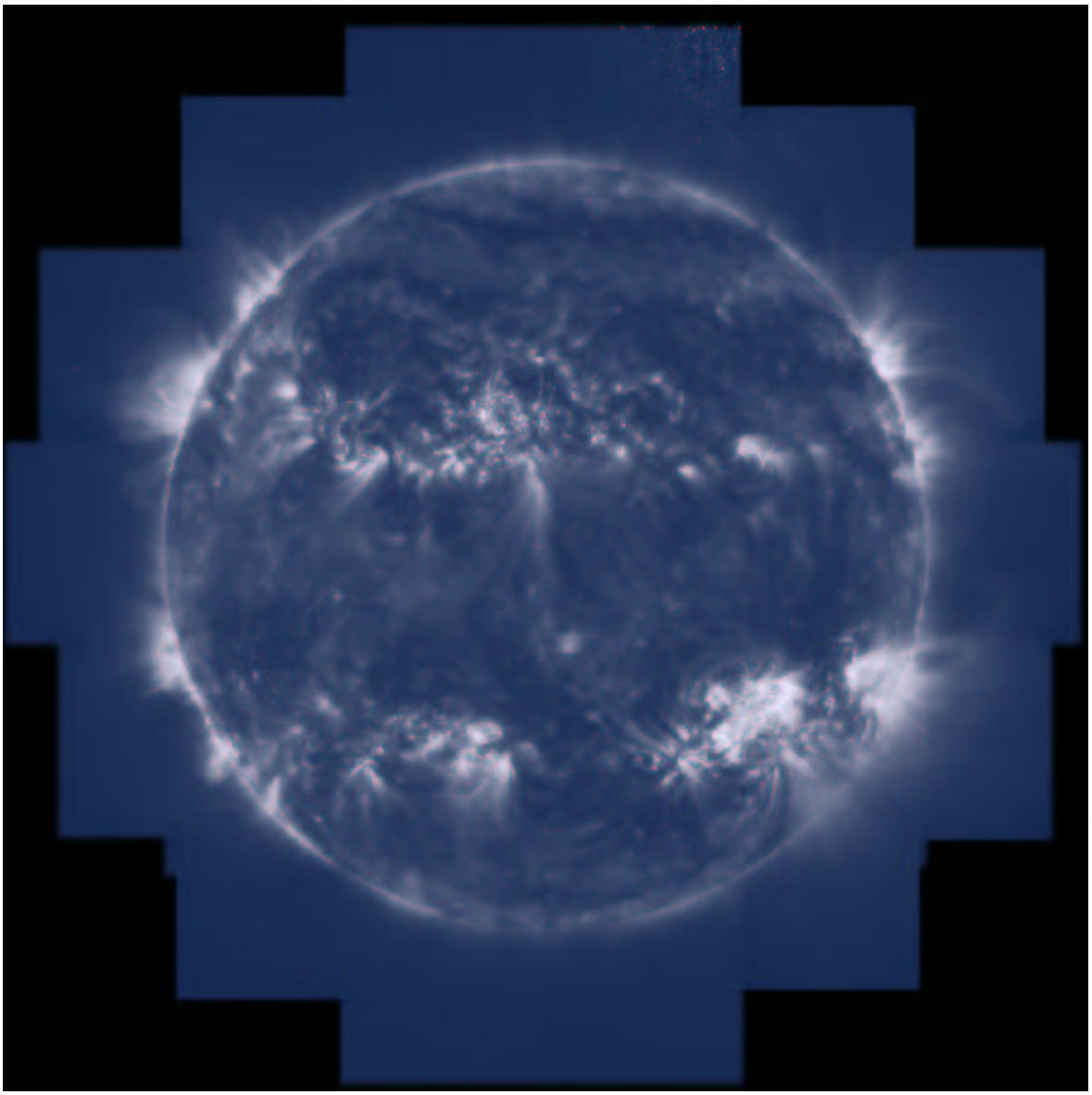

Figure 1.4: Image of the solar disk in Fe IX 171 Å obtained using the Transition Region and Coronal Explorer (TRACE) showing the upper transition region/lower corona at $\sim$ 1,000,000 K. Active regions are visible in two belts north and south of the equator. Plasma loops extending into the corona are also evident.

of TR spectral lines, many of which are optically thick (i.e. have non-negligible opacity) can provide information on mass motions and possible methods of energy transport.

1.1.1 Solar spicules

The edge of the chromosphere is made up of numerous fine jet-like structures known as *spicules*. These features are prevalent in the quiet sun and are significant in both disk and limb observations. The focus of this work is on the modelling of spectral emission from the chromosphere and the TR and so it is useful to consider these spicule structures and their spectral characteristics is some detail.

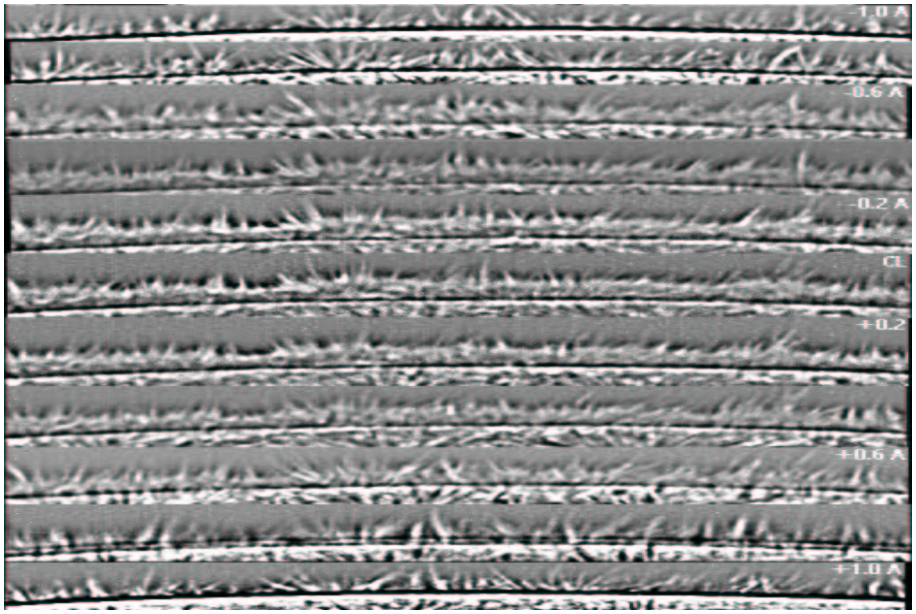

Figure 1.5: Eleven images of spicules at the limb obtained from different regions of the Hα line. The discontinuity between the spicules and the disk is due to the fact that an occulter was used to mask the disk to observe the spicules with the disk observations superimposed below.

Spicules were first described by Secchi (1877) and were named by Roberts (1945). They are jet-like structures with aspect ratios of about 20 (Lorrain and Koutchmy, 1996 – henceforth LK) which rise to heights of around 10,000 $\rightarrow$ 15,000 km with

diameters $\sim 150 \rightarrow 200$ km (eg. Withbroe, 1983; LK; Budnik et al., 1998). Thus they exist at the resolution limit of current instruments (SUMER spatial resolution is ~ 1 arc sec which corresponds to $\sim$ 1000km). The surface coverage of spicules is $\sim 1\%$ (Athay and Holzer, 1982) with about 70,000 of them being present at any one time (LK). They are most commonly observed in chromospheric spectral lines such as Hα (fig 1.5) but also in extreme ultraviolet (EUV) lines from the upper chromosphere and transition region (fig 1.3). Seen in Hα, upon reaching their maximum height their root disconnects from the surface, the proper motion of the cool radiation source becomes downward and they disappear (LK). Lifetimes are $\sim 5 \rightarrow 15$ mins and upward velocities are perceived as (and are generally accepted to be) $\sim$ 25 km/sec. This velocity is inferred from Doppler shifts measured at the limb and so is open to misinterpretation if transverse velocities are present as Beckers suggests. LK add that this velocity is also that perceived by the apparent motion of the spicule head and that the velocity can be much larger ($\sim$ 50-100 km/sec) during the *impulsive phase*.

It is clear that spicule structure, formation and propagation are intimately related to the magnetic field topology, with spicules, as discussed below, appearing within *magnetic elements* (Lorrain and Koutchmy, 1993) at the boundaries of supergranule cells. This link is evident when observing at the limb as well as on disk in the patterns and groupings that are found. A further connection with the magnetic field is evident in coronal holes (regions of very low coronal X-ray emission situated at the poles where the magnetic field lines are open) in the presence of *macrospicules* or *spikes* which extend to $\sim$ 30,000 km above the limb.

Spicules are observable in spectral lines at upper chromospheric and transition region temperatures. Budnik et al. (1998) observed typical "EUV inhomogeneities possibly associated with spicules" growing (if viewed at the limb) horizontally and vertically with increasing emission line temperature until $\sim$ 1–2 x 10^5 K where the structures appear totally diffuse.

Spicules On the Disk

Spicules have photoelectrically controlled spectroscopic characteristics, appearing in absorption when viewed on disk. Spicules at the limb are associated with dark, and

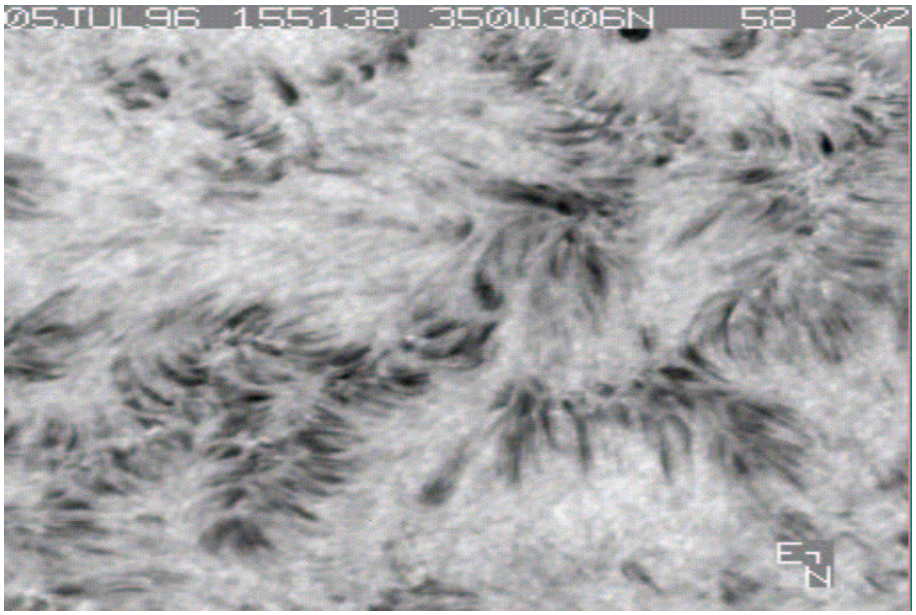

Figure 1.6: A region of the disk seen in Hα showing dark mottle features.

possibly also bright, mottles on the disk (fig. 1.6) which exist at the boundaries of supergranule cells. Dark mottles are absorption features seen against a brighter chromospheric background. Bright mottles are situated at lower heights than dark ones and occur in the same regions where they form groups of around 50 mottles in total forming coarse mottles, *rosettes* or *bushes*.

In mid chromospheric spectral lines, Doppler shifts corresponding to both upflows and downflows are observed whereas in upper chromospheric lines upflows are dominant (Doschek et al., 1976). In contrast, downflows are dominant in TR lines (Athay and Holzer, 1982). These flows provide a key point of interest in the spicule debate on the issues of chromospheric heating, coronal mass and energy balance, and the question of what happens to the TR as a spicule rises beneath it.

The Spectroscopy of Spicules

Spicules are most frequently observed in Hα – they are often referred to as Hα spicules to distinguish them from EUV inhomogeneities. In the visible range they are also often observed in Hβ and calcium lines. Spicules are observed in the upper chromosphere and TR in EUV lines of impurities such as C I $\rightarrow$ C IV. Model based hydrogen densities in spicules have been calculated as $\sim 10^{12}$ cm^{-3} at $T_e \sim 1.5 \times 10^4$ K (Papushev and Salakhutdinov, 1994). Athay & Holzer (1982), however, state that the average hydrogen density within spicules is $\sim 6 \times 10^{10}$ cm^{-3}. Spicules emit spectral radiation at a range of chromospheric and TR temperatures. It is generally assumed

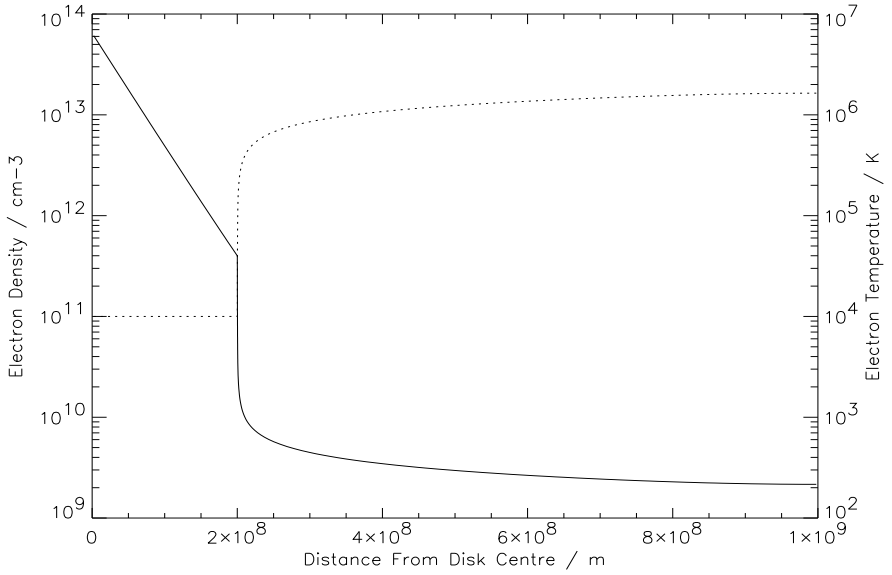

Figure 1.7: Model of the variation of electron temperature (c.f. fig 1.1) and electron density with height according to Vernazza et al. 1981.

that spicules have a 'cool' chromospheric core surrounded by a relatively hot TR sheath. LK suggest in their model, however, a 'hot' core surrounded by a relatively cool sheath (presumably surrounded also by a hot sheath). Instrumental resolution is not yet sufficiently fine to answer this question.

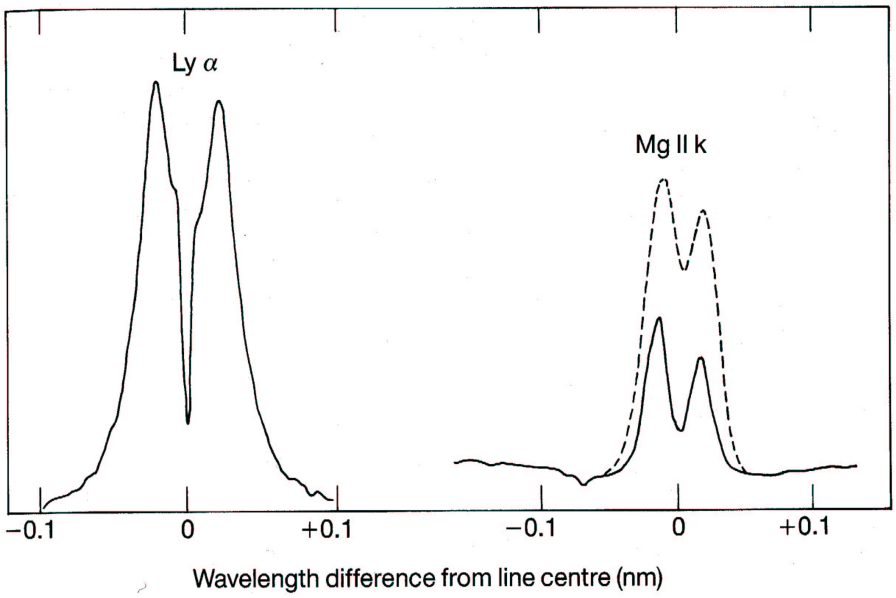

Figure 1.8: Two examples of spectral lines originating in the solar chromosphere. The solid lines correspond to quiet-sun conditions and the dashed line corresponds to active-sun conditions. (Taken from Phillips, 1992).

Many spectral lines originating from spicules and the chromosphere and TR in general are optically thick and can display marked deviation from Gaussian profiles (see fig. 1.8). Furthermore, plasma flow leads to the displacement of lines from their rest wavelengths and possibly also of absorption profiles from emission profiles due to Doppler motion. Thus asymmetries, Doppler shifts, self reversals and broadenings abound in the lines of the chromosphere and TR. A significant contribution to these features is made by large scale non-thermal motions such as rotations. Spicules may be classified as being one of two types (Beckers, 1972): type I – spicules with wide profiles; type II – spicules with narrow profiles. The distinction between these two may be interpreted as being related to rotation. Line profiles are also complicated, especially when viewed on disk, by spicule tilting, by the possible presence of unresolved spicules and the effects of scattered light – both instrumental and due to the inter-spicular medium which also possibly contains unresolved spicule structures.

Papushev and Salakhutdinov (1994) have added to this picture and talk of intricate changes in the Hα profile as the spicule rises. They say that all line profile parameters change by $\sim 30 \rightarrow 40\%$, with $30 \rightarrow 200$s duration during the evolution of the spicule. Furthermore they say that the profiles show asymmetries but that the 'middle' stage is characterised by Gaussian profiles.

Most authors seem to agree that spicule scale heights[1] are $\sim$ 1,500 km ($\sim$ 2,000 km in coronal holes). On the matter of spicule heights, however, there is less coherence. This is largely due to the ambiguous definition of height generally taken to be the maximum height above the limb at which a spicule may be seen. Nevertheless, most authors claim heights to be between 10,000 and 15,000km. The existence of spicules (or, at least, spicule associated inhomogeneity) is more difficult to verify in the case of coronal lines due to the relatively strong background emission. Budnik et al. (1998) used the high resolution SOHO data to identify such inhomogeneities directly by observing the variation of spectral line intensity with position in the vicinity of spicules. Withbroe (1983), on the other hand, approached this issue by comparing observed RMS fluctuations in the intensity with position with the expected statistical fluctuations.

Implications of Spicules to the Mass and Energy Balance of the Corona

As the chromosphere and the TR separate the cool photosphere from the hot corona, and spicules represent mass and energy flux upward from the chromosphere into the corona, it is reasonable to expect spicules to play a significant role in the mass and energy balance of the corona. Simple calculation of the upward mass flux reveals that it is two orders of magnitude greater than that of the solar wind (Athay and Holzer, 1982). Clearly the majority of this material must flow back down again but only 1% need remain to maintain the mass of the corona. Budnik et al. (1998) claim that their SOHO observations mentioned above do show evaporation of spicular material into the corona.

Views on the energy balance question are more varied. Beckers' calculation of

[1] Atmospheric pressure falls off, roughly speaking, as e^{-h/H_s}, where h is the height above the limb and H_s is the scale height

the kinetic energy of a spicule led him to believe that they do not contribute an appreciable amount of energy to the corona. Athay and Holzer (1982), on the other hand, calculated the gravitational potential energy gained by a spicules and found it to be sufficient to power the corona if that energy was dissipated as the spicules descended. They drew on the observed TR downflows as evidence for this. This calculation was, however, dependent on the assumption that spicules rise to greater heights than had been observed ($\sim 5{\times}10^4$km). Withbroe (1983) responded to the Athay and Holzer model by utilising EUV observations to show that spicules do not rise above 15,000 km. He then used DEM analysis to conclude that the observed transition region downflows do not support this model and concluded that spicules are probably not the primary source of heating of the corona.

1.1.2 Solar prominences

It is interesting to consider solar prominences, which are tongues of material that are suspended in the corona since they emit a spectrum at chromospheric temperatures and display optical depth effects. They exist at around 10,000 K, surrounded by 2,000,000 K coronal plasma and consequently have a TR sheath about them. Typical quiescent prominences are 10,000→600,000 km long and 5,000→10,000 km thick and sit at heights up to $\sim$ 50,000 km above the photosphere. Typical lifetimes are around a month. Their formation, structure, stability and ultimate eruption are the focus of much modelling and observational effort and many questions concerning them remain unanswered. Like spicules they appear in absorption when viewed on disk and are visible in fig. 1.2 as dark lanes called filaments. They are also evident in this figure as bright features at the limb. The temperature within the prominence is not sufficient to collisionally excite hydrogen atoms to produce Hα photons and so the presence of prominences in the Hα spectroheliogram seems surprising. The Hα photons arise due to excitation of neutral hydrogen via absorption of Lyman continuum photons from the underlying chromosphere and so do not have anything to do with the actual electron temperatures.

In fig. 1.3 prominences are present despite the fact that this image reveals the

sun at a temperature of $\sim$ 80,000 K – a temperature much greater than that of the prominence itself. This is due to emission from the prominence-corona transition region (PCTR) that exists around the prominence which spans the temperature range of $\sim$ 10,000 $\rightarrow$ 2,000,000 K.

Prominences present many challenging modelling problems since their emission spectrum and energy balance depend critically on photo-electric processes. Thus the details of radiation transport must be carefully computed to model radiative characteristics and power loss.

1.2 Spectral emission from plasmas

Plasmas are made up of atoms, ions and electrons which all radiate via different atomic processes. Understanding such processes is necessary for the modelling of plasmas and the interpretation of spectral data. This involves understanding the electronic structure of atoms and ions and the interactions between particles and photons that couple species, ionisation stages and energy levels to produce the resultant spectrum. This problem is complex but can be handled for a number of regimes.

It is of interest to understand the processes that generate and sustain the solar chromosphere and TR and that drive the processes therein. The principal, if not sole method by which this may be achieved is spectroscopy – i.e. by detailed interpretation and analysis of the light emitted from these regions. If the light emitting mechanisms are to be understood, all the atomic processes that lead to photo-emission must be accounted for. If an ion, A, of charge Z, with outermost electron in excited state i is denoted A_i^{+Z}, then these processes may be summarised as follows:

Radiative processes

1. Spontaneous emission:

$$A_i^{+Z} \rightarrow A_j^{+Z} + h\nu$$

2. photo-absorption:

$$A_j^{+Z} + h\nu \rightarrow A_i^{+Z}$$

3. stimulated emission:

$$A_i^{+Z} + h\nu \rightarrow A_j^{+Z} + h\nu + h\nu$$

4. photo-ionisation:

$$A_i^{+Z} + h\nu \rightarrow A^{+Z+1} + e$$

5. radiative recombination:

$$A^{+Z+1} + e \rightarrow A_i^{+Z} + h\nu$$

6. stimulated recombination:

$$A^{+Z+1} + e + h\nu \rightarrow A_i^{+Z} + h\nu + h\nu$$

7. dielectronic recombination:

$$\begin{aligned} A_i^{+Z+1} + e &\rightleftharpoons A_{j,nl}^{+Z} \\ A_{j,nl}^{+Z} &\rightarrow A_{i,nl}^{+Z} + h\nu \end{aligned} \tag{1.1}$$

Note that h is Planck's constant (6.62618×10^{-34} J s) and ν is the photon frequency in Hz. In dielectronic recombination an ion of charge $Z+1$ captures an electron which loses energy to a bound electron of the ion, exciting it from level i to level j, and leaves the captured electron in a highly excited state denoted nl. At this point the process may reverse in what is called *Auger breakup*, or the inner excited electron may relax via the emission of a photon as indicated. Following this the captured electron may cascade down to a lower level.

If an electron, e, in an energy state i is denoted $e(\varepsilon_i)$, then the collisional processes may be summarised as follows:

Collisional processes

1. Electron impact excitation and de-excitation:

$$A_i^{+Z} + e(\varepsilon_i) \rightleftharpoons A_j^{+Z} + e(\varepsilon_j)$$

2. Electron impact ionisation and 3-body recombination:

$$A_i^{+Z} + e(\varepsilon_i) \rightleftharpoons A_\rho^{+Z+1} + e + e$$

3. Charge exchange recombination:

$$A_i^{+Z+1} + H^0 \rightarrow A_j^{+Z} + p$$

If a plasma is sufficiently dense, as in the solar photosphere, then no radiation can escape except from very close to the outer edge. All photons within the plasma that are emitted are subsequently absorbed. Such a situation is termed *complete thermodynamic equilibrium* and the atom and ion excited state population densities are characterised by *detailed balance*. That is, every individual reaction is balanced by its inverse. In such circumstances the atoms, ions and electrons establish energy distributions with characteristic temperatures. Free particles have a *Maxwellian velocity distribution* given by

$$f(v) = 4\pi \left(\frac{m}{2\pi kT}\right)^{3/2} v^2 exp\left(-\frac{mv^2}{2kT}\right) \tag{1.2}$$

where v is the velocity, m is the mass; k is Boltzmann's constant, and T is the temperature. Bound states of atoms and ions have a Boltzmann distribution. Number densities (populations) of atoms and ions in bound levels i and j with statistical weights ω_i and ω_j, are related by

$$\frac{N_i}{N_j} = \frac{\omega_i}{\omega_j} exp\left(-\frac{E_i - E_j}{kT}\right) \tag{1.3}$$

where E_i and E_j are the energies of levels i and j respectively. For ions of the same species but adjacent ionisation stages, these populations are given by the *Saha-Boltzmann equation*, viz.

$$\frac{N_i^Z}{N_e N_j^{Z+1}} = \frac{\omega_i^Z}{\omega_j^{Z+1}} \frac{h^3}{2\left(2\pi m_e kT\right)^{3/2}} exp\left(-\frac{E_i}{kT}\right) \tag{1.4}$$

The deviation of plasmas from thermodynamic equilibrium is usually due to a deficit in the radiation field. However, there are circumstances where collisional processes

are so efficient that this deficit does not matter and collisional processes alone are sufficient to maintain thermodynamic equilibrium populations. This situation is called *local thermodynamic equilibrium* (LTE). LTE often holds for highly excited states due to their large cross-sections and low transition energies. Low lying levels, however, only achieve LTE at high densities.

Out of thermodynamic equilibrium, detailed balance does not hold. In this case, however, a plasma in equilibrium will have atomic and ion populations satisfying *statistical balance*. That is, the sum of all the processes which populate a level (labelled i) are balanced by those that depopulate it. Thus

$$\begin{aligned}
& \sum_{i'>i} \left[A_{i'\to i} + \int_{line} u(\nu) B_{i'\to i} d\nu + N_e q^{(e)}_{i'\to i} + N_e q^{(p)}_{i'\to i} \right] N_{i'} \\
+ & \sum_{i''<i} \left[\int_{line} u(\nu) B_{i''\to i} d\nu + N_e q^{(e)}_{i''\to i} + N_e q^{(p)}_{i''\to i} \right] N_{i''} \\
+ & N_e N_+ \alpha^{(r)}_i + N_e^2 N_+ \alpha^{(3)}_i + N_e N_+ \int u(\nu) B_{\kappa\to i} d\kappa \\
= & \left[\sum_{i'>i} \left[\int_{line} u(\nu) B_{i\to i'} d\nu + N_e q^{(e)}_{i\to i'} + N_e q^{(p)}_{i\to i'} \right] \right. \\
+ & \sum_{i''<i} \left[A_{i\to i''} + \int_{line} u(\nu) B_{i\to i''} d\nu + N_e q^{(e)}_{i\to i''} + N_e q^{(p)}_{i\to i''} \right] \\
+ & \left. \int u(\nu) B_{i\to\kappa} d\kappa + N_e q^{(e)}_{i\to\varepsilon} + N_e q^{(p)}_{i\to\varepsilon} \right] N_i + \frac{dN_i}{dt}
\end{aligned} \tag{1.5}$$

where

- $A_{i'\to i}$ - spontaneous emission from $i' \to i$
- $u(\nu)B_{i'\to i}$ - stimulated emission from $i' \to i$
- $u(\nu)B_{i\to i'}$ - photo-absorption from $i \to i'$
- $N_e q^{(e)}_{i'\to i}$ - electron collisional de-excitation from $i' \to i$
- $N_e q^{(p)}_{i'\to i}$ - proton collisional de-excitation from $i' \to i$
- $N_e q^{(e)}_{i\to i'}$ - electron collisional excitation from $i \to i'$
- $N_e q^{(p)}_{i\to i'}$ - proton collisional excitation from $i \to i'$

- $\int u(\nu) B_{i\to\kappa} d\kappa$ - photo-ionisation from i
- $N_e q_{i\to\varepsilon}^{(e)}$ - electron collisional ionisation from i
- $N_e q_{i\to\varepsilon}^{(p)}$ - proton collisional ionisation from i
- $N_e N_+ \alpha_i^{(r)}$ - radiative recombination
- $N_e^2 N_+ \alpha_i^{(3)}$ - three body recombination
- $N_e N_+ \int u(\nu) B_{\kappa\to i} d\kappa$ - stimulated recombination

There is such an equation for every level from the ground to $n = \infty$. The solution of these equations yields the *population structure*.

At low densities, such as those in the solar corona, radiation processes control the de-excitation of electrons. *Coronal equilibrium* describes this regime by neglecting the collisional de-excitation term in favour of spontaneous emission. Thus atoms are excited by electron collisions and de-excited by spontaneous radiative decay. They are collisionally ionised by electron impact, and recombine by electron collision. This model neglects collisional de-excitation by assuming that sufficient time elapses between collisions to ensure that excited electrons decay radiatively. Also if an atom is ionised, it has time to recombine before suffering collisions. Furthermore, photo-excitation and photo-ionisation processes are ignored. This is reasonable if the density is sufficiently low.

It is interesting to note that even at the low densities for which the coronal model is valid, highly excited levels may still be collisionally dominated, and so have LTE populations. This may be accounted for within the coronal model by treating such highly excited states as part of the continuum.

Both the solar chromosphere and transition region exist between the thermodynamic equilibrium and coronal regimes where all the radiative and collisional processes come into play. *Collisional-radiative* modelling, first introduced by Bates, Kingston & McWhirter (1962), caters for this middle ground and encompasses the low density coronal and high density LTE regimes. In this model all radiative and *electron* collisional processes are included. However, photo-induced ones (eg. photo-excitation and photo-ionisation) are not.

Collisional-radiative theory recognises the many indirect ways by which highly excited levels can influence the dominant low lying ones. For example, electrons may recombine into a highly excited state and then cascade down to lower levels. Or, following recombination there may be stepwise ionisation. These effects are combined with the direct *state resolved* ionisation and recombination coefficients to produce the collisional-radiative recombination and ionisation coefficients. Also included (Burgess & Summers, 1969) is dielectric recombination to produce *collisional-dielectronic* recombination and ionisation coefficients.

To solve the statistical balance equations the *quasi-equilibrium assumption* is invoked, whereby the highly excited states are assumed to be in equilibrium with the metastable and ground levels. Thus the population densities of all levels apart from the metastable and ground levels, may be found *relative* to the metastable and ground level populations. The quasi-equilibrium assumption follows from consideration of relaxation timescales. In general

$$\tau_{met} \sim \tau_g \sim \tau_{plasma} \sim \tau_{ion} \gg \tau_{ord} \gg \tau_{ee}$$

where these quantities are the metastable, ground, plasma diffusion/dynamic, ion, ordinary excited state and electron-electron equipartition timescales, respectively (see Spitzer, 1956; McWhirter & Summers, 1984; Brooks, 1997). The metastable and ground timescales are similar to the plasma dynamic timescale and so their populations may only be calculated within a transport model which includes these dynamics. However, the ordinary excited state timescale is much smaller than all three and so it is reasonable to assume that at any time the ordinary excited states are in equilibrium with the ground and metastables.

1.3 The problem of opacity

1.3.1 The radiative transfer equation

In the solar chromosphere and transition region the photo-induced effects that are not handled within collisional-radiative theory become important. The plasma is said

to be *optically thick* which means that on average emitted photons have a significant probability of being absorbed before they are able to escape the plasma. This leads to a loss of photons from the line-of-sight. Additionally, absorbed photons affect the population structure which in turn affects the emitted radiation. Thus the system is non-linear and is described by eqs 1.5, coupled with the *radiative transfer* equation

$$\frac{dI_\nu(s)}{ds} = j_\nu(s) - \kappa_\nu(s) I_\nu(s) \tag{1.6}$$

(see Mihalas, 1978, for a complete discussion of radiative transfer theory and Carlsson, 1997, for an eloquent summary of the same.) Here $I_\nu(s)$ is the monochromatic specific intensity (normally called the intensity), $j_\nu(s)$ is the emissivity or emission coefficient, $\kappa_\nu(s)$ is the opacity or absorption coefficient and s is the geometric distance along the ray. These quantities will be defined in more detail in chapter 2. This equation describes the propagation of photons along a ray and must in principle be solved simultaneously with eqs 1.5 if the population structure and/or the emergent intensities along the ray are to be known. The radiation term in eqs 1.5 is $u(\nu)$ which is related to $I_\nu(s)$ as follows:

$$u(\nu) = \frac{h\nu}{c} \int I_\nu(\theta, \phi) d\Omega \tag{1.7}$$

where $d\Omega$ is an element of solid angle. Thus the population structure is no longer dependent merely on local plasma conditions but is coupled into the dynamics and structure of the whole plasma. Consequently radiation transfer plays an important role in determining the structure and energy balance of the solar chromosphere and TR.

Eq. 1.6 implies that the number of photons escaping along the ray is proportional to the opacity and also to the intensity itself. The directional dependence of the intensity follows from the dependence of ds on direction. In the presence of fields (eg. electric, magnetic or velocity), $j_\nu(s)$ and $\kappa_\nu(s)$ may also be directionally dependent.

In a plane-parallel atmosphere the geometrical height, z, which increases outward along the normal of the atmosphere, may be defined. If then the angle between the ray and the normal of the atmosphere is labelled θ and the directional cosine, $\mu = \cos\theta$,

the radiative transfer equation becomes

$$\mu \frac{dI_{\nu\mu}(z)}{dz} = j_\nu(z) - \kappa_\nu(z) I_{\nu\mu}(z) \tag{1.8}$$

It is useful to write this equation in terms of the ratio of the emissivity to the opacity, namely the *source function*, $S_\nu \equiv j_\nu/\kappa_\nu$. Furthermore it is useful to make use of the *optical depth*, τ_ν, which is defined via

$$d\tau_\nu = -\kappa_\nu dz \tag{1.9}$$

With this the radiative transfer equation becomes

$$\mu \frac{dI_{\nu\mu}}{d\tau_\nu} = I_{\nu\mu} - S_\nu \tag{1.10}$$

This is a first order differential equation and thus one boundary condition is required for its solution. In a plane parallel atmosphere there are two boundaries and photons escape through one boundary for negative values of μ and the other boundary for positive values of μ. The conditions for each are $I_\nu^-(0) = 0$ and $I_\nu^+(\tau_{max}) = S_\nu(\tau_{max})$, where the superscripts denote the sign of μ. It follows that the solution of eq. 1.10 is

$$I_{\nu\mu}(\tau_\nu) = \begin{cases} \frac{1}{\mu} \int_{\tau_\nu}^{\infty} S_\nu(t) e^{-(t-\tau_\nu)/\mu} dt & \text{if } \mu > 0 \\ \frac{1}{-\mu} \int_0^{\tau_\nu} S_\nu(t) e^{-(\tau_\nu - t)/(-\mu)} dt & \text{if } \mu < 0 \end{cases} \tag{1.11}$$

This is the *formal* solution of the radiative transfer equation and can only be evaluated if the source function and opacity are known. The source function is dependent on space, frequency and, in essence, upon intensity. The latter dependence follows from that of the emissivity on the upper level population density and will be clarified in chapter 2.

It is useful to define the *contribution function to the intensity*, C_I, which has the defining property

$$I_{\nu\mu}(\tau_\nu) = \int C_I(z) dz \tag{1.12}$$

It follows from eq. 1.11 that

$$C_I(z) = \frac{1}{\mu} S_\nu(\tau_\nu) e^{-\tau_\nu/\mu} \kappa_\nu \tag{1.13}$$

It is important also to consider the difference between *pure absorption* of a photon and *scattering* of a photon. Both are significant in the radiative transfer problem. In pure absorption a photon is absorbed leading to the excitation of an electron which subsequently de-excites via a collisional process. Consequently pure absorption leads to thermal coupling between the point of emission of the photon and that of absorption. In the scattering process a photon is absorbed leading again to the excitation of an electron which this time de-excites via a radiative process. Thus the scattering process does not lead to thermal coupling but, unlike the case of pure absorption, results in a distortion of the emission profile since the photon may be scattered in any direction. Scattering leads to diffusion of photons from the Doppler core where the probability of absorption (i.e. the opacity) is greatest. This in turn leads to the distortion and/or *self-reversal* of emission lines (see fig. 1.8). This effect is termed *partial frequency redistribution* within radiative transfer theory (see sec. 1.3.2). If this is neglected then *complete frequency redistribution* is assumed. This assumption is valid if there are sufficient randomising/redistributive collisions between photo-absorption and re-emission to ensure that there is no dependence of the emission profile on the absorption profile.

1.3.2 Solving the radiative transfer problem

The coupled equations of statistical balance and radiative transfer are currently impossible to solve completely given that in principle their solution involves plasma geometry, flow and even electric and magnetic fields. Advances in computer technology have led to more and more complex treatments of this problem but each solution invokes approximations of either a physical or mathematical nature. These relate to all aspects of the problem, from atomic physics considerations (eg. 2-level atoms – Auer & Paletou, 1994) to the plasma geometries and dynamics (eg. one dimensional static slabs – Carlsson, 1986; Anzer & Heinzel, 1999, 2000). Methods of solution may be grouped into three categories: firstly the methods of *radiative transfer*, secondly *Monte Carlo* computations and thirdly *escape probability* techniques.

Methods of radiative transfer

Radiative transfer methods (see for example Carlsson, 1986; Olson et al., 1986) solve the radiative transfer and statistical balance equations iteratively using a Newton-Raphson technique. The equations are linearised using the Feautrier method (Feautrier, 1964) and solved using *lambda iteration* or *Accelerated Lambda Iteration* (ALI – see Rybicki & Hummer, 1991). Detailed one-dimensional (1D) numerical modelling began with Poland et al. (1971) and Ishizawa (1971). Since then techniques have been extensively developed to include many (i.e. more than two) atomic levels plus continuum states (Heasley & Mihalas, 1976), PRD (eg. Heinzel et al., 1987) and more than one spatial dimension (eg. Paletou et al., 1993). Codes such as MULTI (Carlsson, 1986) and MALI (Rybicki & Hummer, 1991, 1992) have been used by many authors to consider solar and stellar atmospheres as well as solar structures such as prominences and spicules.

Prominences represent a classic radiative transfer problem. Their temperature, density, turbulence and magnetic field are now relatively well known but critical to this understanding was the realisation that observed high excitation temperatures do not reflect the actual electron temperature and density but are the result of non-LTE effects. That is, the incident UV radiation from the chromosphere below has key importance in the ionisation within the prominence. Photo-absorption is thus critical to the energy balance of prominences from the standpoint of ionisation, particularly of hydrogen, and of radiative power loss, particularly from the Lyα and Lyβ lines which are optically thick and strongly self reversed (see fig. 1.8).

The radiative transfer calculations of MULTI and MALI each depend upon an atomic and an atmosphere model. The atomic model contains information on collisional and radiative excitation, de-excitation, ionisation and re-combination processes for all the species to be considered. The atmosphere model contains information on electron temperature and density and elemental abundances. On this basis the calculation consists of iterating back-and-forth between an estimate of the source function and the computation of the associated radiation field until some convergence criterion is reached. This yields key properties for each line including the source function, contribution function, opacity, optical depth and emergent intensity as well as the

excited state population structures for each species considered.

Models such as these are necessary for considering the energy balance in and radiative power loss from optically thick and photo-ionised plasmas. This follows the large oscillator strengths of Lyα and Lyβ, coupled with the abundance of neutral hydrogen in the TR, which lead to these lines being dominant and optically thick radiators. Radiative transfer models are also necessary for the computation of absolute intensities, intensity ratios of lines of different species and emergent line profiles.

The problem with these methods however, is that they are computationally intensive, time-consuming and also usually limited in applicability to particular source configurations which places a limitation on their validity for inhomogeneous plasmas. Plasma geometries considered in this model are usually 1D plane parallel, semi-infinite slabs (eg. Carlsson, 1986; Heinzel et al., 1987; Lanzafame, 1994; Hubeny & Lites, 1995; Goutikakis et al., 1997; Anzer & Heinzel, 1999, 2000) that are stratified with electron temperature and density based on hydrostatic equilibrium (eg. Vernazza et al., 1981, henceforth referred to as VAL), or 1D slabs that are vertically (Heinzel, 1995) or horizontally (Mein et al., 1996) oriented and illuminated, perhaps, by an external source such as the underlying chromosphere and transition region. Two dimensional (2D) models have been developed which allow for transport in two directions but source geometries in such calculations remain simplistic – 2D slabs (Paletou et al., 1993; Auer & Paletou, 1994; Paletou 1996) or isolated prominence threads (Fontenla et al., 1996) for example. In these thread models individual threads are modelled as plane-parallel slabs immersed in a radiation field due to the other slabs.

The problem is that the solar atmosphere has a complex structure and the results from radiative transfer computations may only be interpreted within the simple geometries for which they apply. For example, to approximate the solar transition region as a plane parallel, semi-infinite slab, with electron temperature and density following that of the VAL model, leads to emission at the limb (i.e. looking along the infinite dimension) which is impossible to predict, and zero emission above it. Such a model fails to account for the extension of the transition region into the corona due to the spicule-like structures described in sec. 1.1.1. Moreover, these techniques provide no way to extract information directly from observations about optical depths

or plasma structure. This is not to say that radiative transfer based diagnostics of plasmas are not made. Heinzel et al. (1996) performed a complex diagnostic of prominences using 140 models computed by Gouttebroze et al. (1993). However, plasma parameters deduced from such diagnostics can only be interpreted with reference to a preconceived plasma configuration.

Monte Carlo methods

Monte Carlo techniques for radiative transfer have been used in astrophysics to model plasmas with random geometries such as the Lyα forest (Zheng et al., 1998) and optically thick *blobs* in stars and the interstellar medium (Code & Whitney, 1995). Such techniques have also been used to model solar phenomena such as coronal loops (Guttebroze et al., 1986; Wood & Raymond, 2000). The advantage of Monte Carlo radiation transfer simulations is that they naturally account for arbitrary illumination and multiple scattering in complex geometries.

In the Monte Carlo method photon scattering is described by using random numbers to sample from probabilistic interaction laws in order to follow photons as they scatter through a medium.

Again, however, approximations are necessary and in this case there is a trade off between geometric complexity and detail in the line formation process. More specifically, these calculations model random walks of photons and so purely describe the scattering process. Many subtleties arising from absorption such as the influence of opacity on the source and contribution functions and ionisation balance are not included. Consequently these methods are restricted to moderate optical depths. This is not a severe restriction since many astronomical lines have low but non-zero optical depths. However, Monte Carlo techniques are model based and so, as with the radiative transfer techniques, they provide no means by which plasma parameters may be extracted directly from observations independently of a geometric model.

Escape probability techniques

The escape probability was introduced by Holstein (1947) and associated expressions have since been developed by a number of authors (McWhirter, 1965; Irons, 1979; Hummer & Rybicki, 1982: Kastner & Kastner, 1990). The effects of opacity in solar spectral lines have been studied on a number of occasions using such methods (Jordan, 1967; Doschek et al., 1976; Doyle & McWhirter, 1980). Jordan established the technique of using branching ratios of lines arising from a common upper level to extract information on opacities directly from spectral observations. Doyle & McWhirter subsequently developed this same technique to study opacity at the solar limb and their work included a simple model of predicted line ratios from the region on-disk up to the limb. Many authors have constructed models of both laboratory and astrophysical plasmas using escape probability techniques (Doyle & McWhirter, 1980; Orrall & Schmahl, 1980; Keenan & Kingston ,1986; Brooks et al., 2000).

Escape probability methods, which will be discussed in detail in subsequent chapters, rely on assumptions that simplify the source function term in eqs 1.5 and 1.6. These assumptions naturally decouple and linearise the equations. Consequently these methods provide approximate solutions to eqs 1.5 and 1.6 in a moderate optical depth regime. This approach has the virtue of practicality. As stated above, escape probability expressions provide diagnostic tools to extract plasma parameters directly from observations. Furthermore they have the potential to be used in plasma models of arbitrary geometric complexity. For example, Orral & Schmahl (1980) used *attenuation factors* (identical in principle to escape probabilities) to account for opacity within prominence models. These models consisted of resolved slabs or unresolved threads. The radiative transfer computations (as stated above) consider individual threads in isolation and model them as plane parallel slabs.

1.4 Thesis overview

The techniques described above all rely on a set of assumptions which differ between and within the three approaches presented. The validity of any solution, assuming any

numerical schemes employed are effective (efficiently or otherwise), is entirely dependent on the prescribed problem – that is the nature of the assumptions made. It does not matter that a solution is numerically sophisticated if the underlying assumptions are invalid.

This work aims to investigate the relatively simple escape probability techniques for solving the coupled sets of equations of statistical balance and radiative transfer (eqs 1.5 and 1.6). The assumptions that underpin such techniques will be tested in order to asses the extent of their validity and the nature of their invalidity as the regime is entered within which they break down.

In chapter 2 an overview of the techniques will be given and their coupling to simple atmosphere models will be demonstrated in comparison with data from the SOHO-SUMER spectrometer. In chapter 3 these methods will be reviewed to consider inhomogeneous models in a consistent way and to assess the modification to the source function due to opacity. In chapter 4 the effects of line blending will be analysed and in chapter 5 the influence of structure and plasma flows will be examined. Then in chapter 6 the SUMER observations discussed in chapter 2 will be re-visited from a model and diagnostic perspective. The improved escape probability techniques will be used to re-assess simple empirical models and to extract information on optical depths and structure directly from observations in a manner that is model independent.